

## Single-photon emission from pyramidal quantum dots: The impact of hole thermalization on photon emission statistics

A. Malko, D. Y. Oberli, M. H. Baier, E. Pelucchi, F. Michelini, K. F. Karlsson, M.-A. Dupertuis, and E. Kapon  
*Ecole Polytechnique Fédérale de Lausanne (EPFL), Laboratory of Physics of Nanostructures, CH-1015 Lausanne, Switzerland*

(Received 6 April 2005; revised manuscript received 6 September 2005; published 22 November 2005)

We report an experimental study of the emission statistics of excitonic complexes from a single quantum dot and their temperature dependence. The single photon emission from the exciton ground state is shown to persist up to 80 K. The deterioration of single photon statistics is attributed to new biexciton emissions, which emerge in the vicinity of the main single-exciton peak at rising temperatures. We identify these biexcitonic states as being formed by either one hole or two holes occupying excited states and analyze their specific polarization and power-dependent signature.

DOI: [10.1103/PhysRevB.72.195332](https://doi.org/10.1103/PhysRevB.72.195332)

PACS number(s): 78.67.Hc, 42.50.Dv

The rapidly evolving field of quantum information technology relies on nonclassical emission sources capable of emitting single photons at predetermined times and with well-established spectral and temporal characteristics. These sources are required for the implementation of quantum computation<sup>1,2</sup> and quantum communication protocols.<sup>3</sup> An atom considered as a two-level quantum system emits spontaneously antibunched photons when it is excited because the emission of one photon resets the system in its ground state and a subsequent emission cannot occur immediately afterwards. A single semiconductor quantum dot (QD) is often described as the solid-state analog of an atom since three-dimensional confinement results in a discrete energy spectrum. Unlike an atom, however, a QD is incorporated in a solid-state environment that introduces carrier-lattice interaction. Hence, the atomic-like picture of the unperturbed ground state, which can serve as a quantum emitter<sup>4</sup> at low enough temperature (around 10 K), partially breaks down at elevated temperatures when excited states are being occupied and when electron-phonon interaction broadens the optical transitions. The interaction with the solid-state environment is thus expected to also have an impact on the statistics of photons emitted by QD excitons, particularly at elevated temperatures. An understanding of this impact is particularly important for the realization of practical solid-state single photon emitters operating at sufficiently high (e.g.,  $T > 77$  K) temperatures.

The temperature dependence of the features of single photon emission from semiconductor QDs has been left so far largely unexplored; there are only few studies of high temperature ( $>40$  K) photon emission statistics from epitaxially grown QDs.<sup>5</sup> In this paper we report on an experimental study of the temperature dependence of the photon antibunching from single pyramidal InGaAs/AlGaAs QDs. Extending our previous work,<sup>6</sup> we demonstrate single photon statistics of the exciton ( $X$ ) emission from 10 K up to 80 K. This is the highest temperature for which photon antibunching is reported for such a material system. By using single photon correlation measurements combined with a quantitative analysis of the emission spectra, we find that emission from other transitions related to the QD ground state, such as biexciton ( $2X$ ) and positively charged exciton ( $X^+$ ) cannot

cause a disappearance of photon antibunching. Instead, we identify the presence of the transitions involving holes in excited states as the origin of a broadband background that gradually sets in as the temperature is raised. It serves as a source of photons that leads to the observed degradation of the photon antibunching from the  $X$  line.

The investigated QDs were grown by low-pressure organo-metallic chemical vapor deposition (OMCVD) on  $2^\circ$  off-(111)B GaAs substrates that were pre-patterned with an array of inverted pyramids with a  $5\ \mu\text{m}$  pitch. The sample resulted from a growth sequence of 45-nm-thick  $\text{Al}_{0.75}\text{Ga}_{0.25}\text{As}$  layer (etch-stop layer), 130 nm  $\text{Al}_{0.55}\text{Ga}_{0.45}\text{As}$ , 70 nm  $\text{Al}_{0.3}\text{Ga}_{0.7}\text{As}$ , the 0.5 nm  $\text{In}_{0.1}\text{Ga}_{0.9}\text{As}$  quantum well (QW) layer, 70 nm  $\text{Al}_{0.3}\text{Ga}_{0.7}\text{As}$ , and 130 nm  $\text{Al}_{0.55}\text{Ga}_{0.45}\text{As}$ . Thicknesses refer to the growth on a planar (100) substrate; layers are nominally undoped. The growth on a nonplanar substrate yields a lens-shaped InGaAs QD at the bottom of the inverted pyramid.<sup>7</sup> In addition, a vertical QWR is formed at the center of the pyramid due to Ga segregation. After the growth, the GaAs substrate was removed using selective wet chemical etching, resulting in an array of up-right standing pyramids. The substrate removal step is used to increase the photon extraction efficiency by a factor of about  $10^3$ , which makes the pyramid suitable for low-power optical measurements.<sup>7</sup>

The optical emission properties of the pyramidal QDs were investigated by a Hanbury-Brown and Twiss (HBT) setup for the photon correlation measurements combined with a microphotoluminescence ( $\mu\text{PL}$ ) setup for the PL studies as described in Ref. 8. The sample was mounted in a He-flow cryostat and kept at a temperature of 10 K. The sample was excited either by the beam of a continuous-wave laser operating at 532 nm or of a pulsed Ti:sapphire laser emitting at 740 nm; it was focused to  $\sim 1\ \mu\text{m}$  spot by a microscope objective ( $\text{NA}=0.55$ ). The emitted light was collected by the same objective, then split by a 50/50 beam-splitter into separate arms and directed toward two spectrometers for spectral filtering before being detected by single photon counting avalanche photodiodes (APDs). The outputs of the APDs served as start and stop signals for a modulation domain analyzer acting as a correlator. This unit allowed for the measurement of the histogram displaying the raw number

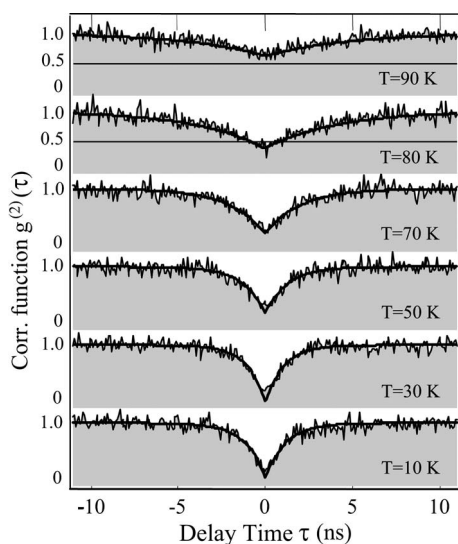


FIG. 1. Second-order correlation function  $g^{(2)}(\tau)$  of  $X$  emission line at different temperatures. Solid lines: fits of the measured correlation curves including temporal response of the HBT. The fitted decay times corresponding to temperatures increasing from 10 to 90 K are 1.2, 1.1, 1.3, 2, 3.5, and 4 ns.

of start-stop events  $c(\tau)$  as a function of the time delay  $\tau$  after renormalization, this yields the second-order correlation function  $g^{(2)}(\tau)$ . The time resolution of HBT setup was 0.7 ns. The  $\mu$ PL spectra were acquired with a CCD camera and the spectral resolution was 100  $\mu$ eV. For the time-resolved PL measurements, we used a microchannel-plate—photomultiplier tube that yielded a time resolution better than 50 ps.

Figure 1 shows the normalized second-order correlation curves  $g^{(2)}(\tau)$  obtained from the emission of a neutral  $X$  confined in a single QD at different temperatures. The measurements were performed at a low-power excitation intensity, which for the temperatures 10–50 K corresponds to an average number of electron-hole pairs  $N_{eh} \ll 1$ , as checked from the power dependence of the spectra (not shown). All traces exhibit clear dips at  $\tau=0$ , indicating photon antibunching. A zero value of  $g^{(2)}(0)$  is a direct proof of the single photon nature of the emitted light. The experimental values of  $g^{(2)}(0)$  are limited by the finite time-resolution of HBT setup. In order to account for the time resolution we fitted measured count distributions with the correlation function  $g_i^{(2)}(\tau) = 1 - (1-A)\exp(-|\tau|/t_m)$  that was convolved with a Gaussian time distribution of 700 ps width. Parameter  $A$  corresponds to the uncorrelated emission in the measurements and  $t_m$  is the characteristic decay time of the antibunching trace. The resulting curves  $g_i^{(2)}(\tau)$  shown in Fig. 1 (solid lines) yield zero-delay dips smaller than 0.5 for all temperatures below 80 K, demonstrating the predominant emission of single photons.

The fitted functions  $g_i^{(2)}(\tau)$  do not vanish at a zero delay because of a background signal that is superimposed on each  $X$  emission line. As the sample’s temperature is raised, this contribution becomes larger as evidenced by our fits that yield an increasing value of  $A$  from 0.11 at 10 K to 0.41 at 80 K. In order to elucidate the origin of this background

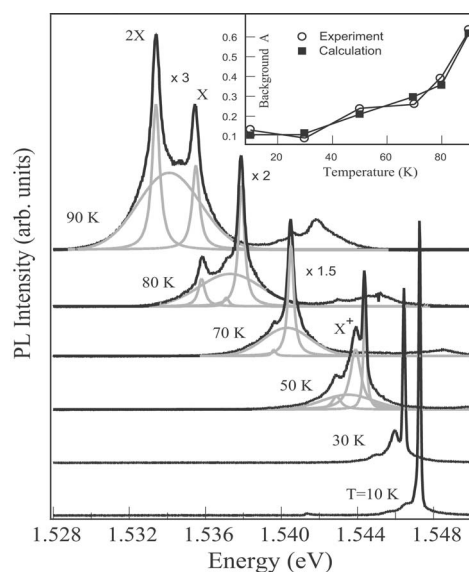


FIG. 2.  $\mu$ PL spectra of the same pyramidal QD performed under identical experimental conditions as the temporal correlation measurements of Fig. 1. Gray curves—decomposition of the measured spectra (black lines) into its components as marked on the figure. Spectra are offset for clarity. Inset: Values of the experimental background “A” as measured from correlation curves on Fig. 1 (open circles) and calculated from spectra (black squares).

signal, we display in Fig. 2 the corresponding  $\mu$ PL spectra that were recorded under the same experimental conditions (temperature and excitation power). At a sufficiently low excitation power, the spectrum taken at a temperature of 10 K consists of a narrow  $X$  line and of a weak background. Increasing the excitation power leads to the appearance of several other lines (spectra not shown) due to the effect of state filling. Similar occurrences arise in the spectra of Fig. 2 that are recorded at higher temperatures and at a low excitation power; several other lines in addition to  $X$  and a stronger background contribute to the spectra. One of these lines was identified as a  $2X$  by its dependence with excitation power and by photon correlation measurements, which showed a pronounced bunching behavior with the  $X$  line.<sup>9,10</sup> The weaker emission line appearing with a redshift of 0.6 meV with respect to the  $X$  emission at  $30 \leq T \leq 50$  K has, however, a pronounced antibunching signature with  $X$ ; it is attributed to the  $X^+$  transition.<sup>10</sup> In addition, a broadband background signal overlaps with all the lines and constitutes a large fraction of the spectral emission at elevated temperatures.

In order to evaluate the role of the background in the correlated photon emission we performed a line shape analysis to isolate its contribution to the spectra. We use Lorentzian line shapes for all excitonic lines and a Gaussian profile for the broadband background. We assume that the emission deteriorating photon antibunching of the  $X$  line arises from this background and that it has Poissonian statistics. We evaluated the signal to background ratio  $\rho = S/(S+B)$  for each spectrum, where  $S$  stands for the signal (pure  $X$  emission) and  $B$  for the background count rates, as described in Ref. 11, and calculated values of  $g_i^{(2)}(0) = A$  for each spectrum

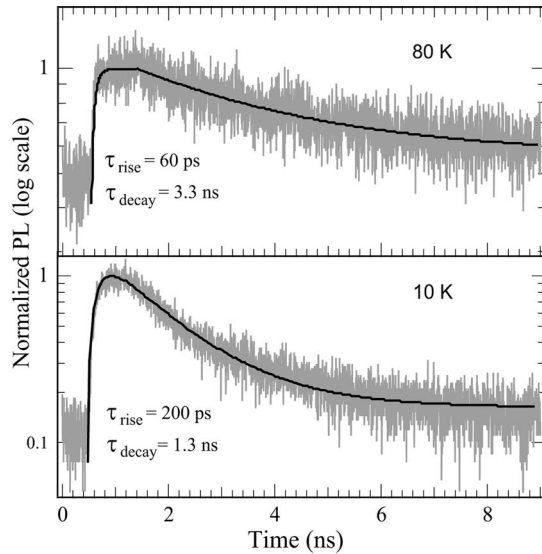


FIG. 3. Semilogarithmic plot of photoluminescence time decay of the X line at the temperatures of 10 and 80 K.

taken. We find that the values of  $A$  are close to the ones measured from the experimental antibunching curves (see the inset to Fig. 2). Furthermore, we emphasize that the contribution of other emission lines to the signal at X wavelength is negligible as evidenced by the weak overlap of the Lorentzian lines. In the case of the  $X^+$  emission which leaks into the detection region (see 50 K spectrum) no effect on the photon antibunching of the X transition is expected. In a QD, excitons such as  $X$  and  $X^+$  (or  $X^-$ ) cannot exist at the same time; therefore, their emission will exhibit a strong photon antibunching.<sup>8,12,13</sup> We verified that the cross-correlation trace of these two lines was characterized by a pronounced antibunching trace with  $g^{(2)}(0) < 0.5$ , thus excluding the possibility of  $X^+$  emission mixing with that of  $X$ . Therefore, we deduce that the broad spectral background is the source of uncorrelated photons causing the temperature dependence of the antibunching dip.

In addition to reducing the depth of the antibunching curves, raising the temperature leads to a monotonous widening of the antibunching notches as it is seen from the correlation traces in Figure 1. In the regime of low-pump intensity, the measured decay time  $t_m$  corresponds directly to the radiative lifetime,  $T_{\text{rad}}$  of the X transition. At temperatures  $T > 50$  K we observe the signature of the 2X emission in the spectra, indicating that although the excitation power is kept constant, the time-averaged number of  $e$ - $h$  pairs confined in the dot increases. For those conditions, the  $t_m$  sets a lower limit of  $T_{\text{rad}}$ .<sup>13</sup> The values of  $t_m$  span a range from 1.2 ns at 10 K to 3.6 ns at 80 K pointing to an increase of the PL radiative decay time.

In order to corroborate this interpretation we independently measured the X decay time by pumping the same single QD with a mode-locked Ti:sapphire laser. The resulting decays of the PL intensity at X are shown in Fig. 3 for two different temperatures. The data are analyzed by solving rate equations for a three-level system, where the QD ground state is the intermediate level. It results in a biexponential dependence of the intensity:  $I_{\text{PL}}(t) \propto \exp(-t/\tau_{\text{decay}})$

$-\exp(-t/\tau_{\text{rise}})$ . Here  $\tau_{\text{rise}}$  is the capture time of the carriers into the QD and  $\tau_{\text{decay}}$  is the QD X lifetime. At 10 K, the experimental data are well fitted by this model yielding a rise time of 200 ps and a decay time of 1.3 ns, and are consistent with the previously proposed picture of the  $e$ - $h$  pairs that are fed by VQWR into the QD and then recombining from the ground state.<sup>7</sup> At 80 K, a decrease in the rise time is found ( $\tau_{\text{rise}} < 60$  ps); then the intensity remains constant, which indicates state filling of the ground state. This is corroborated by the appearance of the 2X line in the corresponding  $\mu$ PL spectrum. A modification of the fit is necessary to account for the plateau. Its width is determined by the increased diffusion length of the carriers along the VQWR before they are captured by the QD. Emiliani *et al.*<sup>14</sup> also showed a tenfold increase of the carrier diffusion length for analogous QWR-QD coupled structures and explained it by thermal excitation of the carriers out of the local potential minima formed by interface fluctuations. The decay time is fitted to 3.3 ns.

The increase in the QD luminescence decay time is qualitatively explained by a distribution of hot holes over several excited states that are closely spaced in energy. Numerical calculations taking into account the shape of the confinement potential predict a compact spacing of the hole energy levels, a minimum of three hole states confined in the dot and all three of them residing within a 10 meV range. Due to the significant phonon broadening at elevated temperatures that is comparable to this interlevel separation, the transitions involving excited hole levels are not anymore resolved and merge into a featureless background. The spectral weight of these transitions is significant at the X emission line as attested by the spectral analysis presented in Fig. 2. Because the radiative rates of these transitions are considerably smaller than the radiative rate of the X emission, a corresponding increase of the decay time of the X emission arises when the temperature is progressively raised. Additionally, the decay time is also directly affected by the occupation probability of the hole in the ground state, which is progressively reduced by an increase of temperature. Since the PL decay time is inversely proportional to the occupation probability, the PL decay time is expected to rise with a temperature increase as a quasi-thermal equilibrium is approached in the later stage of the carrier dynamics. Brasken *et al.*<sup>15</sup> also observed a similar dependence of the luminescence decay time with temperature in InGaAs/GaAs stressor-formed dots. They modeled, however, the increase in the decay time solely by accounting for the later effect assuming that a thermal population was established among the hole states. We note that experiments performed on dots with a much larger energy level separation resulted in a nearly temperature-independent QD luminescence decay time (Ref. 16), which is fully consistent with our explanation.

So far, the optical transitions associated with either an X,  $X^+$  or 2X were simply regarded as Lorentzian broadened lines. All the experimental evidences can be consistently explained if the broadband spectral background is a source of uncorrelated photons. It is well known that increased interaction of confined excitons with acoustical phonons leads to the deviation of a zero-phonon line from its Lorentzian profile with the appearance of acoustical phonons sidebands at el-

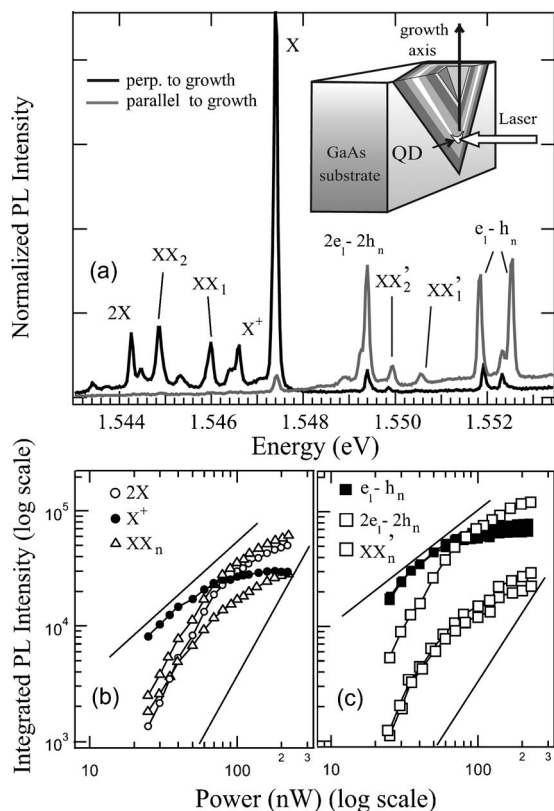


FIG. 4. (a)  $\mu$ PL spectra of a QD taken in a cleaved edge geometry. Black line—measured in polarization perpendicular to the growth axis, gray line—parallel to it. Emissions from different excitonic complexes are marked on the figure.  $2X$  labels the biexciton emission,  $XX_n$  and  $XX_n'$  are the biexcitonic emissions associated with excited hole states. Inset: picture of the cleaved edge excitation geometry. Intensity dependences with excitation power of the lines lying energetically lower than  $X$  (b) and higher than  $X$  (c). The straight lines indicate either a linear or a quadratic dependence on these logarithmic plots of the PL intensity vs excitation power.

evated temperatures.<sup>17</sup> However, phonon scattering with the  $X$  does not alter the single photon emission statistics. For a photon antibunching to occur only the fact that photons are emitted one by one is relevant. Therefore, a nonzero value of  $g^{(2)}(0)$  should involve a radiative process either with a cascade of several photons or with an emission of several photons at the same time.<sup>18</sup>

In order to uncover the origin of the background as a source of uncorrelated photons we performed  $\mu$ PL measurements of the same sample in a different geometry. Instead of using the back-etched sample and of collecting the luminescence from the apex of the pyramid, which only gives access to the emission polarized in the plane perpendicular to the pyramid's (or growth) axis, we used a "cleaved" sample geometry as illustrated in the inset of Fig. 4. The sample was cleaved in a plane containing the growth direction and illuminated from the cleaved edge in order to analyze the polarization of the emission lines in the direction perpendicular and the one parallel to the growth axis. In Fig. 4(a) we show the  $\mu$ PL spectra for which the polarization is analyzed along these two orthogonal directions. Detecting perpendicularly polarized emission (at 10 K), we observe a sharp emission

line ( $X$ ) at 1.5474 eV and a multitude of weaker lines on its low-energy side. For parallel-polarized emission, several other peaks were observed in an energy range of 1.5 to 5.5 meV above the  $X$  emission energy. We tentatively assign these transitions to the recombination of an electron in the ground state ( $e_1$ ) and a hole in one of the excited states ( $h_2, h_3$ , etc.).

In order to affirm this assignment, we model within the single-particle approximation the energy eigenstates of generic pyramidal quantum dots having similar sizes and shapes to our QD. We find that the calculated eigenenergies of the hole states ( $h_1, h_2, h_3$ , etc.) are indeed consistent with the energy spacing of the optical transitions that are about 5 meV above the  $X$  line. In addition, the model predicts that these optical transitions are nominally forbidden and that they become optically active because of the valence band mixing and of the low mesoscopic symmetry in quantum nanostructures.<sup>19</sup> For the same reasons, optical transitions that did not conserve the electron and hole subband indices were observed in V-groove QWRs and were similarly characterized by a strong polarization anisotropy.<sup>20</sup> Furthermore, we calculated the oscillator strengths of the ( $e_1-h_n$ ) transitions and thereby confirmed the strong polarization anisotropy that is experimentally observed. Since the model and the results of the calculation go beyond the scope of this experimental study, we will defer their presentations to a forthcoming article.<sup>21</sup>

As the weak intensity of the transitions shown on Fig. 4(a) did not allow us to perform cross-correlation studies between different lines, we had to resort to excitation power dependence measurements in order to clarify their origin. These results are presented on Figs. 4(b) and 4(c) for lines energetically lower and higher than the  $X$ , respectively. As depicted, the integrated PL intensity of these lines exhibits either a linear increase (slopes in the range: 0.85 to 1.18) or a superlinear increase (slopes in the range: 1.95 to 2.2) with increasing excitation density. Taken together with the observed relationship between the onset and the saturation, the linear (quadratic) power dependence of the intensity reflects the excitonic (biexcitonic) origin of these emission lines.

Based on these evidences and on the energetic positions of the lines, which are consistent with the calculated hole-state separation, we assign the peaks at 1.5519 and 1.5525 eV to excitonic transitions associated with the single-particle states ( $e_1-h_n$ ;  $n \neq 1$ ). Similarly, we ascribe two other groups of peaks to biexcitonic transitions: one of them is on the low-energy side of the exciton peak ( $X$ ) and the other one is on its high-energy side. These biexcitonic transitions are depicted schematically in Figs. 5(b) and 5(c): they are associated with an excited biexciton state formed by two electrons in state  $e_1$  and two holes in state  $h_1$  and  $h_n$ , respectively. When the biexciton state (with the configuration: ( $e_1-e_1-h_1-h_n$ )) decays by radiative recombination, it can follow two radiative channels that are characterized by a distinct photon energy depending on whether a hole in  $h_1$  or in  $h_n$  recombines with an electron in single-particle state  $e_1$ . The group of two peaks lying on the low-energy side of the  $X$ , at 1.5448 and at 1.546 eV, corresponds to the radiative recombination of an electron in state  $e_1$  with a hole in state

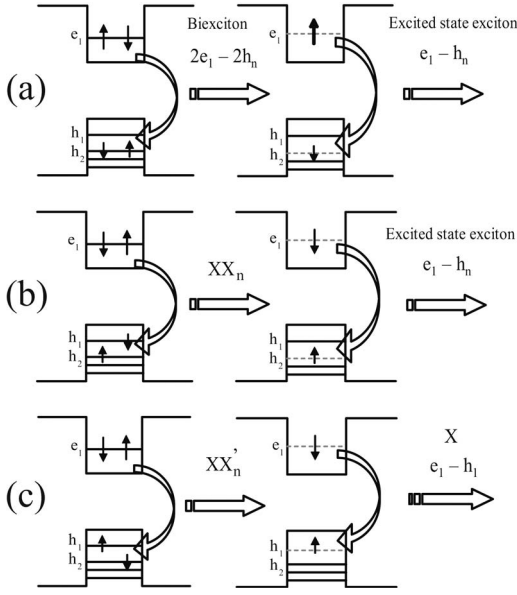


FIG. 5. Schematic representation of the cascade emission of biexcitonic states associated with the configurations  $(e_1-e_1-h_2-h_2)$  in (a) and  $(e_1-e_1-h_1-h_2)$  in (b) and (c). In the second configuration, there are two radiative channels for each of the spin multiplets of the biexcitonic state.

$h_1$  [see Fig. 5(b)]. The group of two peaks lying on the high-energy side of  $X$ , at 1.5498 and at 1.5506 eV corresponds to the radiative recombination of an electron in state  $e_1$  with a hole in state  $h_n$  [see Fig. 5(c)]. Our assignment is based on an analysis of the energy spacing between the two peaks, the presentation of which is deferred to a subsequent section.

The peak at 1.5494 eV and its shoulders on the low-energy side are tentatively assigned to biexcitonic transitions associated with two electrons in state  $e_1$  and two holes in state  $h_n$  [see Fig. 5(a)]. This later assignment is essentially justified by the biexciton binding energy of the main peak at 1.5494 eV, which is expected to have the same magnitude as that of the regular biexciton at 1.5443 eV ( $2X$ ). We applied the standard definition of the biexciton binding energy as the energy separating the peaks  $X$  and  $2X$ . For this QD, it amounts to 3.2 meV ( $B_{2X}$ ). Since the biexciton state formed with two electrons and two holes respectively in the same single-particle state is a singlet state, only one line is predicted for each of the configuration  $(e_1-e_1-h_n-h_n)$  and is indeed observed.

In this next section, we present the analysis of the energy spacing of the biexcitonic peaks. We specifically discuss a biexciton that corresponds to a configuration  $(e_1-e_1-h_1-h_n)$  and we consider one of the spin-multiplet states of this biexciton. A relationship between the photon energies that are emitted in the cascade recombination of this biexciton can be derived as follows. The biexciton energy  $E(XX_n)$ , is equal to the sum of the single-particle energies [ $E(e_1)$  and  $E(h_i)$  for electron and hole, respectively] and of the Coulomb interaction energy  $E_C^S$ ; its expression is  $E(XX_n) = E(e_1) + E(e_1) + E(h_1) + E(h_n) - E_C^S(XX_n)$ , where the label  $S$  in  $E_C^S$  stands for the total spin quantum number of the biexcitonic state.<sup>22</sup> The energy of the second photon emitted in the cascade pro-

cess of Fig. 5(c) is simply  $h\nu_2 = h\nu(X) = E(e_1) + E(h_1) - E_C(X)$ , where  $E_C(X)$  is the Coulomb interaction energy between the electron in state  $e_1$  and the hole in state  $h_1$ . We then simply find the energy of the first photon emitted in the cascade process  $h\nu_1 = E(XX_n) - h\nu_2$ , which is rewritten as  $h\nu_1 = E(e_1) + E(h_n) + E_C(X) - E_C(XX_n)$ . In the same way, we derive the energy of the first photon emitted in the cascade process of Fig. 5(b):  $h\nu_1' = E(e_1) + E(h_1) + E_C(X_n) - E_C(XX_n)$ , where  $E_C(X_n)$  is the Coulomb interaction energy between an electron in state  $e_1$  and a hole in state  $h_n$ . From these expressions, we simply get the energy separation of the biexcitonic lines as  $\Delta E = h\nu_1 - h\nu_1' = E(h_n) - E(h_1) + E_C(X) - E_C(X_n) = h\nu_2' - h\nu_2$ . The last term in the previous expression is exactly equal to the spectral separation between the  $X$  peak and one of the excitonic transitions labeled  $(e_1-h_n)$ . With the expression of the energy separation at hand it becomes nearly straightforward to associate the pair of spectral peaks that results from the first stage of the radiative cascade of a given biexcitonic state: e.g. the pair of peaks that are labeled  $(XX_n)$  and  $(XX_n')$  in the PL spectra of Fig. 4(a) corresponds to  $h\nu_1$  and  $h\nu_1'$ , respectively.

The above picture remains unchanged though the Coulomb interaction can couple different configurations together: e.g., a spin-multiplet state of the configuration  $(e_1-e_1-h_1-h_2)$  is mixed by the Coulomb interaction with the same spin-multiplet states of other configurations  $(e_1-e_1-h_1-h_n)$ . Although we did not evaluate numerically the amount of configuration mixing, we could expect it to be important when the typical energy scale of the Coulomb interaction becomes comparable to the energy separation of hole single-particle states. This situation might arise in the present dot, which has closely spaced hole states; thus, one cannot ascribe a given biexcitonic peak to a unique configuration.

Let us now consider the implications of the spin-multiplicity of a biexciton made of a configuration  $(e_1-e_1-h_1-h_n)$ . For the  $C_{3v}$  symmetry of pyramidal quantum dots, the hole states  $h_n$  are doubly degenerated like  $h_1$  is. The electronic configuration  $(e_1-e_1-h_1-h_n)$  is thus associated with a spin quadruplet state because the holes occupy different single-particle states.<sup>23</sup> The Coulomb interaction lifts the degeneracy of the two-pair state into a spin singlet (with total spin quantum number of 0) and a spin triplet (with total spin quantum number of 1). As a result of the energy splitting of the two-pairs eigenstate, we expect to observe two spectral lines for each spin multiplet of the biexciton in the configuration  $(e_1-e_1-h_1-h_n)$ . We note that the weaker peaks on the low energy side of each of the main peaks labeled  $XX_n$  are probably good candidates for the biexcitonic lines originating from the spin-triplet biexciton state. A firmer assignment of these peaks must await, however, a quantitative estimation of the exchange energy for this particular QD.

The observed multiplets of biexcitonic transitions are at the origin of the appearance of the background and of the deterioration of the antibunching at elevated temperatures. Pyramidal QDs that we studied have only one confined electronic level, which is twofold degenerate. The configuration  $(e_1-e_1-h_1-h_1)$  gives rise to two distinct optical transitions, labeled  $2X$  and  $X$  in Fig. 4(a), as the result of the radiative recombination of the biexciton state in a cascade process.<sup>9</sup> At

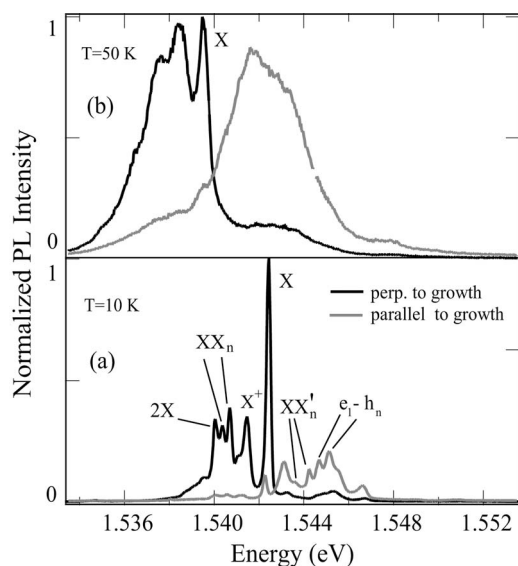


FIG. 6.  $\mu$ PL spectra of a QD measured in cleaved edge geometry at the temperatures of 10 (a) and 50 K (b).

rising temperatures, a non-negligible holes population is present on higher-lying energy states due to the interplay between thermionic excitation and absorption. In Fig. 6 we present  $\mu$ PL measurements taken at different temperatures for another QD of the same sample. As previously shown in Fig. 5(a), several lines are clearly visible at 10 K though the lines are somewhat broader and the spacing between the excitonic transitions ( $e_1-h_n$ ) and the X peak is reduced to about 3 meV. As the temperature is raised, the biexcitonic transitions both on the high- and low-energy side of the X peak increase their contribution in comparison to the X line and, at 50 K, they merge into broad and featureless peaks due to phonon broadening effects, see spectrum in Fig. 6(b). Most importantly, these peaks start to spectrally overlap with the X peak at rising temperatures. This creates a situation propitious to bunching of the  $2X-X$  type in the emission statistics because the decay of an excited biexcitonic state can involve in the last stage of the cascade the emission of a photon at the energy of the X peak. Even a small portion of such events will lead to a strong bunching signature<sup>12,24</sup> and then to the partial disappearance of the antibunching dip when these sequential recombination events are accounted for.

Single photon characteristics in the study of photon emission statistics persisted up to a temperature of 80 K (see Fig. 2) while on Fig. 6(b) broadband peaks are already dominating the spectrum at 50 K. We simply attribute this difference to a slight difference in the size of the dot that was used for the antibunching study. This is inferred from the spectral position of the weaker excitonic peaks ( $e_1-h_n$ ) in Fig. 2, which are about 5 meV higher in energy than the X peak as compared to the 3 meV separation observed in Fig. 6.

Another mechanism that could contribute involves a simultaneous photon emission. Because of the strong interaction of the confined excitons with phonons the picture of the  $2X-X$  cascade as a sequence of recombination events of a two-level system must be revised. Instead, a correlated emission from a three-level system mediated by the phonon interactions has to be considered. This process will undoubtedly produce concurrent emissions and be evidenced by bunching statistics with a maximum bunching value of 2,<sup>18</sup> therefore leading to a deterioration of the antibunching signature in the emission statistics of X.

In summary, we have shown that single photon emission from single pyramidal QDs persisted up to a temperature of 80 K, pertaining to their use as single photon emitters. By combining the technique of photon correlation with  $\mu$ PL spectroscopy we identified the spectral signatures of several excitonic and novel multiexcitonic complexes including the charged exciton line  $X^+$ . We further evaluated the influence of the multiexcitonic complexes on the statistics of the photons emitted by the QD at elevated temperatures. We found that biexcitons associated with the configuration ( $e_1-e_1-h_1-h_n$ ) were the main source of photons that were temporally and spectrally correlated with the emission of the exciton in its ground state (X). Given the importance of developing functional single photon source, a thorough understanding of the carrier interactions with the solid-state environment is needed in order to fully assess the potential of quantum dots for single photon emission at liquid nitrogen temperature and above it.

This work was supported by a grant from the National Center for Competence in Quantum Photonics Research funded by the Swiss National Science Foundation (NCCR-Quantum Photonics). The authors thank Alok Rudra for his assistance in the MOCVD growth.

<sup>1</sup>E. Knill, R. Laflamme, and G. J. Milburn, *Nature (London)* **409**, 46 (2001).

<sup>2</sup>C. Santori, D. Fattal, J. Vuckovic, G. S. Solomon, and Y. Yamamoto, *Nature (London)* **419**, 594 (2002).

<sup>3</sup>N. Gisin, G. Ribordy, W. Tittel, and H. Zbinden, *Rev. Mod. Phys.* **74**, 145 (2002).

<sup>4</sup>C. Santori, M. Pelton, G. Solomon, Y. Dale, and Y. Yamamoto, *Phys. Rev. Lett.* **86**, 1502 (2001); V. Zwiller, H. Blom, P. Jonsen, N. Panev, S. Jeppesen, T. Tsegaye, E. Goobar, M. E. Pistol, L. Samuelson, and G. Björk, *Appl. Phys. Lett.* **78**, 2476 (2001).

<sup>5</sup>R. Mirin, *Appl. Phys. Lett.* **84**, 1260 (2004); K. Sebal, P. Michler, T. Passow, D. Hommel, G. Bacher, and A. Forchel, *ibid.* **81**, 2920 (2002).

<sup>6</sup>M. H. Baier, E. Pelucchi, E. Kapon, S. Varoutsis, M. Gallart, I. Robert-Philip, and I. Abram, *Appl. Phys. Lett.* **84**, 648 (2004).

<sup>7</sup>A. Hartmann, Y. Ducommun, K. Leifer, and E. Kapon, *J. Phys.: Condens. Matter* **11**, 5901 (1999); K. Leifer, A. Hartmann, Y. Ducommun, and E. Kapon, *Appl. Phys. Lett.* **77**, 3923 (2000).

<sup>8</sup>A. Malko, M. H. Baier, E. Pelucchi, D. Y. Oberli, D. Chek-al-kar, and E. Kapon, *Appl. Phys. Lett.* **85**, 5715 (2004).

- <sup>9</sup>E. Moreau, I. Robert, L. Manin, V. Thierry-Mieg, J. M. Gérard, and I. Abram, *Phys. Rev. Lett.* **87**, 183601 (2001).
- <sup>10</sup>A. Malko, M. H. Baier, E. Pelucchi, D. Chek-al-kar, D. Y. Oberli, and E. Kapon, *Physica E (Amsterdam)* **26**, 194 (2005); M. H. Baier, A. Malko, E. Pelucchi, D. Chek-al-kar, D. Y. Oberli, and E. Kapon (unpublished).
- <sup>11</sup>R. Brouri, A. Beveratos, J. P. Poizat, and P. Grangier, *Opt. Lett.* **25**, 1294 (2000).
- <sup>12</sup>A. Kiraz, S. Falth, C. Becher, B. Gayral, W. V. Schoenfeld, P. M. Petroff, L. Zhang, E. Hu, and A. Imamoglu, *Phys. Rev. B* **65**, 161303(R) (2002).
- <sup>13</sup>C. Becher, A. Kiraz, P. Michler, A. Imamoglu, W. V. Schoenfeld, P. M. Petroff, L. Zhang, and E. Hu, *Phys. Rev. B* **63**, 121312(R) (2001).
- <sup>14</sup>V. Emiliani, F. Intonti, C. Lienau, T. Elsaesser, R. Notzel, and K. H. Ploog, *Phys. Rev. B* **64**, 155316 (2001).
- <sup>15</sup>M. Brasken, M. Lindberg, M. Sopanen, H. Lipsanen, and J. Tulkki, *Phys. Rev. B* **58**, R15 993 (1998).
- <sup>16</sup>S. Fafard, S. Raymond, G. Wang, R. Leon, D. Leonard, S. Charbonneau, J. L. Merz, P. M. Petroff, and J. E. Bowers, *Surf. Sci.* **361/362**, 778 (1996).
- <sup>17</sup>L. Besombes, K. Kheng, L. Marsal, and H. Mariette, *Phys. Rev. B* **63**, 155307 (2001); E. A. Muljarov and R. Zimmermann, *Phys. Rev. Lett.* **93**, 237401 (2004).
- <sup>18</sup>R. Loudon, *The Quantum Theory of Light* (Clarendon Press, Oxford, 1988).
- <sup>19</sup>G. Bester, S. Nair, and A. Zunger, *Phys. Rev. B* **67**, 161306(R) (2003).
- <sup>20</sup>E. Martinet, M.-A. Dupertuis, L. Sirigu, D. Y. Oberli, A. Rudra, K. Leifer, and E. Kapon, *Phys. Status Solidi A* **178**, 233 (2000); M. A. Dupertuis, E. Martinet, D. Y. Oberli, and E. Kapon, *Europhys. Lett.* **52**, 420 (2000).
- <sup>21</sup>F. Michelini, M. A. Dupertuis, and E. Kapon (unpublished).
- <sup>22</sup>The Coulomb correlation energy  $E_C^S$  depends on the total spin because of the contribution of the exchange interaction between the holes in states  $h_1$  and  $h_n$ .
- <sup>23</sup>A. Barenco and M. A. Dupertuis, *Phys. Rev. B* **52**, 2766 (1995).
- <sup>24</sup>The amount of bunching for  $2X-X$  cascade is determined by the ratio of the probability of the  $X$  emission after the  $2X$  emission occurred to that of  $X$  emission in a steady-state.